Rapid Communications

Quasi-one-dimensional nanoscale modulation as sign of nematicity in iron pnictides and chalcogenides

Dheeraj Kumar Singh,[1,2,3,*] Alireza Akbari,[2,3,4,†] and Pinaki Majumdar[1]

[1]*Harish-Chandra Research Institute, HBNI, Chhatnag Road, Jhunsi, Allahabad 211019, India*

[2]*Asia Pacific Center for Theoretical Physics, Pohang, Gyeongbuk 790-784, Korea*

[3]*Department of Physics, POSTECH, Pohang, Gyeongbuk 790-784, Korea*

[4]*Max Planck POSTECH/Korea Research Initiative (MPK), Gyeongbuk 376-73, Korea*

(Received 16 May 2018; revised manuscript received 15 October 2018; published 26 November 2018)

Impurity scattering is found to lead to quasi-one-dimensional nanoscale modulation of the local density of states in iron pnictides and chalcogenides. This "quasiparticle interference" feature is remarkably similar across a wide variety of pnictide and chalcogenide phases, suggesting a common origin. We show that a unified understanding of the experiments can be obtained by simply invoking a fourfold symmetry breaking d_{xz}-d_{yz} orbital splitting, of a magnitude already suggested by the experiments. This can explain the one-dimensional characteristics in the local density of states observed in the orthorhombic nematic, tetragonal paramagnetic, as well as the spin-density-wave and superconducting states in these materials.

DOI: 10.1103/PhysRevB.98.180506

The intriguing anisotropic electronic properties of iron pnictides [1] are reflected in transport measurements [2–4], optical conductivity [5], angle-resolved photoemission spectroscopy (ARPES) [6], and scanning tunneling microscopy (STM) [7]. It is not unexpected in a state having a broken fourfold rotational symmetry such as the spin-density-wave (SDW) state or the orthorhombic "spin nematic" state, but the lattice anisotropy does not explain a splitting of ≈60 meV between the d_{xz} and d_{yz} orbitals [8,9]. The orbital splitting (OS) actually persists into the high-temperature tetragonal phase [9]. This suggests that the OS, rather than the orthorhombic symmetry or magnetic order, could be the key player in electronic anisotropy. A similar OS exists in various phases [10–15] of the chalcogenide including the superconducting state. The energy scale of FeSe splitting, and its orbital character, have been contrasted with those of the pnictides, with some suggestions of a momentum-dependent, i.e., nonuniform, splitting. Unlike the pnictides where the degeneracy of bands dominated mainly by d_{xz} and d_{yz} orbitals at the X or Y points is lifted at low temperature, the OS for chalcogenides may also exhibit a sign reversal. Some have reported it to be of an entirely different nature, OS between $d_{xz/yz}$ and d_{xy} [16,17].

Valuable insight into electronic anisotropy can be obtained through the "quasiparticle interference" (QPI) phenomena which basically probe the spatial variation of the local density of states (LDOS), due to impurities in the medium, using spectroscopic imaging (SI) STM [18]. A remarkable characteristic of the QPI common to the SDW state, the orthorhombic nematic phase, and the tetragonal paramagnetic phase, in some of the pnictides is the occurrence of quasi-one-dimensional real-space LDOS modulation with a material-dependent length scale [7,19,20]. A corresponding momentum-space structure in the form of almost parallel ridges is aligned along a direction reciprocal to the ferromagnetic direction in the SDW state, or the b axis in the orthorhombic phase for pnictides. Similar momentum- and real-space structures have been reported in the superconducting phase of chalcogenides [11]. This suggests a common origin of the anisotropy in the electronic structure, rather than in specific ordering tendencies.

In the SDW state, the orbital occupancy difference that can result from the electronic reconstruction is $n_{xz} - n_{yz} \sim 0.1$ [21], which corresponds roughly to an energy splitting of 50 meV. According to the experiments, the OS observed above the Néel temperature T_N can be as large as ∼60 meV [6], therefore it is natural to explore the consequences of this "orbital bias" in studying the SDW state as well, ignored in earlier work, which may have led to their failure in reproducing the one-dimensional (1D) characteristics with a correct orientation and length scale [22–25]. Such a term should assume further importance, beyond magnetic anisotropy, in the electron-doped region of the SDW state where the magnetic moments are small, and magnetic-order-induced band reconstruction is less pronounced.

Above T_N, a nonzero OS has been attributed to the spin-driven nematic order with $\langle \mathbf{S_i} \cdot \mathbf{S_{i+x}} - \mathbf{S_i} \cdot \mathbf{S_{i+y}} \rangle \neq 0$, where the average magnetic moment $\langle \mathbf{S_i} \rangle = 0$, because of the frustration caused by the presence of second-nearest-neighbor exchange coupling [26–28]. It is not clear enough how this mechanism will support the OS term of a similar strength below T_N in the SDW state, which we find necessary to explain the 1D QPI characteristics. In another scenario, OS may also originate from the ferro-orbital order [29–32] caused by spin-orbital mode coupling, which can be responsible for an OS larger than what is expected as merely induced by the SDW state. The behavior of orbital order appears to have a remarkable similarity to some of the manganites where the

*dheeraj@postech.ac.kr

†alireza@apctp.org

orbital order precedes the magnetic order as temperature is lowered [33], except that the lattice distortion is small enough in iron-based superconductors to account for such a large OS.

In this Rapid Communication, we suggest a unified explanation for the common QPI characteristics of different phases of iron-based superconducting systems. Our proposal is that an explicit OS term in the Hamiltonian is crucial irrespective of phases. Thus, our point of departure in the standard five-orbital Hamiltonian is the OS term,

$$\mathcal{H}_{\rm orb} = -\frac{\delta}{2}\sum_{i\sigma}\left(d^{\dagger}_{ixz\sigma}d_{ixz\sigma} - d^{\dagger}_{iyz\sigma}d_{iyz\sigma}\right). \tag{1}$$

Here, $d^{\dagger}_{i\gamma\sigma}$ ($d_{i\gamma\sigma}$) is the creation (annihilation) operator for an electron in the d_γ orbital with spin σ at site i. The impurity scattering effects that generate the spatial LDOS modulations, i.e., QPI patterns, are handled via a t-matrix approach on the mean-field states of this theory.

Our key results are listed as follows: (i) We obtain nearly 1D LDOS modulations, i.e., real-space QPI patterns, a feature observed universally across various phases. (ii) For the five-orbital model used in this work, the wavelength of the modulations is $\sim 8a_{\text{Fe-Fe}}$, in excellent agreement with STM measurements for the SDW state of $Ca(Fe_{1-x}Co_x)_2As_2$ [7]. (iii) We identify two large energy windows of size $\sim$60 meV where the LDOS modulation is one dimensional. For the SDW state it is oriented along the antiferromagnetic direction as observed in the experiment. This happens when the energy of the d_{xz} orbital is lower than that of d_{yz}. (iv) The key factor responsible for all the findings above is the OS term which leads to the upward or downward shift of either set of electron pockets located around $(0, \pm\pi)$ or $(\pm\pi, 0)$. Combined with a large spectral density due to nearby band extrema, it results in a strongly momentum-dependent spectral density along the constant energy contours, yielding the anisotropic patterns.

We start to analyze the QPI in the superconducting (SC) phase. The mean-field (MF) Hamiltonian written in the Nambu formalism is

$$\mathcal{H}_{\rm sc} = \sum_{\mathbf{k}}\Psi^{\dagger}_{\mathbf{k}}\begin{pmatrix}\hat{\varepsilon}_{\mathbf{k}} & \hat{\Delta}_{\mathbf{k}}\\ \hat{\Delta}^{\dagger}_{\mathbf{k}} & -\hat{\varepsilon}_{\mathbf{k}}\end{pmatrix}\Psi_{\mathbf{k}}, \tag{2}$$

where the electron field operator is defined as $\Psi^{\dagger}_{\mathbf{k}} = (\phi^{\dagger}_{\mathbf{k}\uparrow}, \phi_{-\mathbf{k}\downarrow})$ with $\phi^{\dagger}_{\mathbf{k}\uparrow} = (d^{\dagger}_{\mathbf{k}1\uparrow}, \ldots, d^{\dagger}_{\mathbf{k}5\uparrow})$ where subscripts 1–5 denote the five d orbitals $d_{3z^2-r^2}$, d_{xz}, d_{yz}, $d_{x^2-y^2}$, and d_{xy} in the same order. Here, $\hat{\varepsilon}_{\mathbf{k}}$ is a 5×5 hopping matrix [34], and $\hat{\Delta}_{\mathbf{k}}$ is a 5×5 pairing matrix. The effective s^{+-} pairing state is mediated by the antiferromagnetic fluctuations generated by the interplay of Fermi-surface nesting and the on-site Coulomb interaction, and the interaction part of the Hamiltonian is given by

$$\mathcal{H}_{\rm int} = U\sum_{\mathbf{i},\mu} n_{\mathbf{i}\mu\uparrow}n_{\mathbf{i}\mu\downarrow} + \left(U' - \frac{J}{2}\right)\sum_{\mathbf{i},\mu<\nu} n_{\mathbf{i}\mu}n_{\mathbf{i}\nu} - 2J\sum_{\mathbf{i},\mu<\nu}\mathbf{S}_{\mathbf{i}\mu}\cdot\mathbf{S}_{\mathbf{i}\nu} + J'\sum_{\mathbf{i},\mu<\nu,\sigma} d^{\dagger}_{\mathbf{i}\mu\sigma}d^{\dagger}_{\mathbf{i}\mu\bar{\sigma}}d_{\mathbf{i}\nu\bar{\sigma}}d_{\mathbf{i}\nu\sigma}. \tag{3}$$

Here, the respective terms represent intraorbital, interorbital density-density, Hund's coupling, and pair-hopping energy ($J' = J$) in the given order. For simplicity, we consider only intraorbital pairing with the same and isotropic gap elements, $\Delta_0 \cos k_x \cos k_y$ (in general, the SC gap is also expected to be anisotropic [35]). We set $\Delta_0 = 20$ meV and the band filling is fixed at $n = 6.1$. The complete Hamiltonian is given by $\mathcal{H}_{\rm orb} + \mathcal{H}_{\rm sc} + \mathcal{H}_{\rm imp}$, where $\mathcal{H}_{\rm imp} = \sum_{\mu\sigma} V_{\rm imp} d^{\dagger}_{j\mu\sigma}d_{j\mu\sigma}$ accounts for a nonmagnetic deltalike impurity scatterer present at site j. The modulation caused in the LDOS by the impurity term is calculated within the t-matrix approximation and only orbitally diagonal scattering is retained [36].

The MF Hamiltonian in the SDW state is obtained after standard decoupling of the on-site terms in Eq. (3) as

$$\mathcal{H}_{\rm SDW} = \sum_{\mathbf{k}\sigma}\Psi'^{\dagger}_{\mathbf{k}\sigma}\begin{pmatrix}\hat{\varepsilon}_{\mathbf{k}} + \hat{N} & \operatorname{sgn}\bar{\sigma}\,\hat{W}\\ \operatorname{sgn}\bar{\sigma}\,\hat{W} & \hat{\varepsilon}_{\mathbf{k}+\mathbf{Q}} + \hat{N}\end{pmatrix}\Psi'_{\mathbf{k}\sigma}. \tag{4}$$

Here, the new electron field operator is defined as $\Psi'^{\dagger}_{\mathbf{k}\sigma} = (\phi^{\dagger}_{\mathbf{k}\sigma}, \phi^{\dagger}_{\mathbf{k}+\mathbf{Q}\sigma})$ with the ordering wave vector $\mathbf{Q} = (\pi, 0)$. Matrices $\hat{N}$ and $\hat{W}$ are obtained in a self-consistent manner. The band filling in this case is $n = 6.0$. We chose the intraorbital Coulomb interaction $U = 0.96$ eV and Hund's coupling $J = 0.25U$ while the pair-hopping interaction $J' = J$ and interorbital density-density interaction parameter $U' = U - 2J$ are determined by the standard relations. Our choice of U yields a net magnetization $m = 0.3$ consistent with the experiments [37].

Now we discuss the QPI results. Throughout, the impurity potential strength is set to be $V_{\rm imp} = 200$ meV, and the mesh size of 300×300 in the momentum space is used. Real-space QPI or LDOS modulation is obtained using the property of the Fourier transform. We set the OS to be $\delta = 60$ meV unless stated otherwise. QPI in the nematic phase is calculated by setting the SC order parameters to zero with band filling $n = 6.0$ (for different OS values, see the Supplemental Material [38]).

To understand QPI patterns in the orthorhombic nematic or tetragonal paramagnetic phase as shown in Figs. 1(d)–1(i), we first examine the quasiparticle spectral functions [Figs. 1(a)–1(c)]. An important consequence of a nonzero δ is the difference in size of the two sets of pockets around $(\pm\pi, 0)$ and $(0, \pm\pi)$ with a large but nonuniform spectral density along both of them [see Fig. 1(a)]. Note that the pockets are on the verge of disappearance near $\omega \sim -100$ meV. The spectral density is larger along these pockets because of the nearby extrema. As a result, $\mathbf{q}_1$ and $\mathbf{q}_2$ are the important scattering vectors, and among them those aligned parallel to either of the x or y directions are the most prominent ones, as they connect the regions dominated by the same orbital. This follows straight from the fact that only intraorbital scattering is allowed. The main consequence to be described below is the orientation of LDOS modulation along either x or y.

For $\omega \sim -100$ meV, $\mathbf{q}_1$ associated with the electron pockets around $(0, \pm\pi)$ should be the dominant scattering vector despite the fact that $\mathbf{q}_2$ also connects the pockets having a larger spectral density. That is because of the availability of a larger phase space as the electron pockets are bigger in contrast with those around $(\pm\pi, 0)$. In particular, $\mathbf{q}_1$'s which are parallel to the x direction should dominate the QPI patterns.

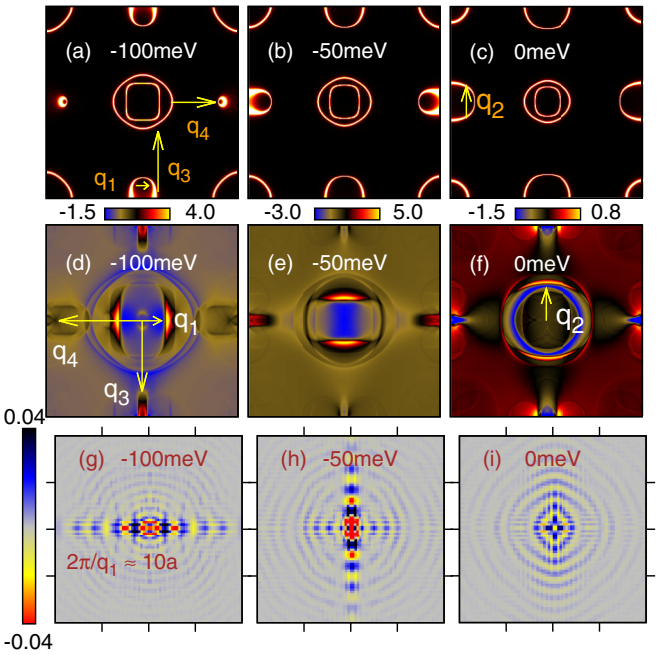

FIG. 1. Results in the nematic state for orbital splitting $\delta = 60$ meV: (a)–(c) show the behavior of contours of constant energies (CCEs) for the quasiparticle energy $\omega = -100, -50, 0$ meV in the (k_x, k_y) plane. $\mathbf{q}_1$ and $\mathbf{q}_2$ are intrapocket scattering vectors associated with the electron pockets around $(0, \pm\pi)$ and $(\pm\pi, 0)$, respectively. Intrapocket scattering vectors for the hole pockets around (0,0) are not shown. $\mathbf{q}_3$ and $\mathbf{q}_4$ are the interpocket scattering vectors. (d)–(f) For most ω, three parallel rodlike structures exist in the momentum space QPI, where the outer peaks are positive and the inner peak is negative. Since the orientation of these rodlike structures also changes near $\omega \sim -60$ meV, the orientation of 1D LDOS modulation (g)–(i) also changes from x to y. Note: Here and hereafter the momentum space plots are in the units of π/a with a range $[-1, 1]$; and the real-space (xy-plane) plots are in the units of a with a range $[-40, 40]$. LDOS modulation shown for 80×80 size with the impurity atom located at the center, with the calculation done for a 300×300 lattice size.

When energy increases through $\omega \sim -60$ meV, contours of constant energies (CCEs) move away from the band extrema, and the smaller pocket around $(\pm\pi, 0)$ grows while the bigger ones around $(\pm\pi, 0)$ do not show much change. However, the spectral density along the pockets around $(\pm\pi, 0)$ becomes larger in comparison to that along the pocket around $(0, \pm\pi)$. Thus, $\mathbf{q}_2$ instead of $\mathbf{q}_1$ is now the dominant scattering vector. CCEs move further away from the band extrema, when ω increases and crosses $\sim$0 meV. Then, the QPI patterns are expected to become nearly isotropic and featureless.

As anticipated, a larger spectral density along the sides parallel to the major axis of elliptical CCEs around $(\pm\pi, 0)$ and $(0, \pm\pi)$ results in the dominance of $\mathbf{q}_1$ or $\mathbf{q}_2$ in the momentum-space QPI patterns, which is shown in Figs. 1(d)–1(f). When $\omega < -60$ meV, $\mathbf{q}_1$ leads to a nearly parallel rodlike positive peak structures at $\sim(\pm\pi/5, 0)$ running parallel to $q_x \sim \pm\pi/5$. A negative peak structure along $q_x \sim 0$ is also seen. When ω decreases and crosses -60 meV, $\mathbf{q}_2$ instead of $\mathbf{q}_1$ becomes relevant and the patterns are rotated by 90°. Near

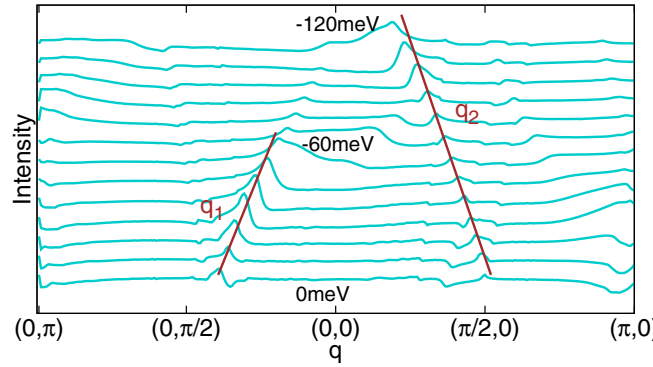

FIG. 2. QPI along the high-symmetry directions in the nematic state, for different energies, from $\omega = 0.0$ meV (bottom curve) to $\omega = -120$ meV (top curve) with an energy step of 10 meV. The brown and red curves are a guide to the eye for scattering vectors $\mathbf{q}_1$ and $\mathbf{q}_2$.

$\omega = 0$, QPI is featureless. A recent SI-STM on $FeSe_{1-x}S_x$ also reports an isotropic QPI patterns for positive ω [40].

Figures 1(g)–1(i) show the real-space QPI in the immediate vicinity of the impurity atom on an 80×80 lattice size for better visibility though the calculation was done for a 300×300 lattice size. Nearly 1D LDOS modulation is obtained over a wide energy window of $\sim$100 meV centered around $\omega \approx -60$ meV. As expected, modulating directions are orthogonal to each other, i.e., along x and y for $\omega \lesssim -60$ meV and $\omega \gtrsim -60$ meV, respectively. The wavelength of modulation for $\omega = -100$ meV is $\lambda_n \sim 10a_{\text{Fe-Fe}}$, which is close to $\sim 13a_{\text{Fe-Fe}}$ observed in the nematic state of NaFeAs [20]. Note that QPI dispersion shows an almost linear dependence for $\mathbf{q}_1$'s and $\mathbf{q}_2$'s, which are centered around $(0, \pi/4)$ and $(\pi/4, 0)$, respectively (Fig. 2).

Figures 3(a) and 3(b) show a calculated quasiparticle spectral function and QPI in the momentum space in the

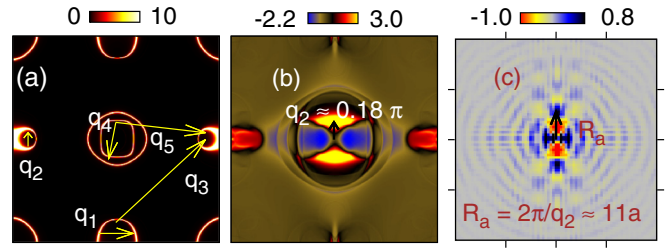

FIG. 3. Results in the s^{+-} superconducting state for $\Delta_0 = 20$ meV, and quasiparticle energy $\omega = -88$ meV in the presence of orbital splitting $\delta = 60$ meV: (a) Quasiparticle spectral function in the (k_x, k_y) plane, (b) momentum-space QPI in the (q_x, q_y) plane, and (c) real-space QPI. The pockets in (a) at $(\pm\pi, 0)$ are very small with a highly anisotropic spectral density distribution along them. The intrapocket scattering vector $\mathbf{q}_2$ is mainly responsible for the features observed near $(0, 0)$ in the momentum-space QPI pattern. These consist of three parallel rodlike structures, the outer ones with a positive peak and the inner one with a negative peak. Real-space QPI consists of two bright spots separated by a distance of $\sim 11a_{\text{Fe-Fe}}$ as observed in the experiments [39]. The ranges for all the quantities are as in Fig. 1.

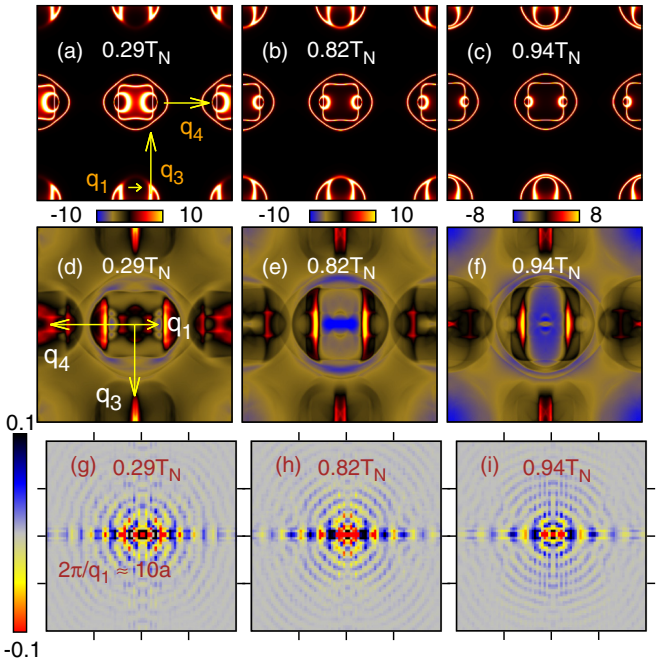

FIG. 4. (a)–(c) show the quasiparticle spectral function for -100 meV in the $(\pi, 0)$ SDW state for various temperatures. Total magnetization is $m_{\text{tot}} = 0.3$. The resulting momentum-space pattern with three parallel rodlike structures is along a direction reciprocal to the ferromagnetic chain and LDOS modulation with wavelength $\sim 8a$–$10a$ with a small change in temperature. The range for all the quantities are as in Fig. 1.

SC state for energy $\omega = -88$ meV, respectively. The LDOS modulation obtained by using the Fourier transform is shown in Fig. 3(c). As can be seen, a nanostructure in the vicinity of impurity atom centered around $(0, 0)$ exists with orientation along y, which can change with energy to x. The distance between two consecutive bright spots is $\sim 11a_{\text{Fe-Fe}}$. STM measurement in the SC state of $FeSe_{1-x}S_x$ with broken fourfold rotation symmetry reports a scattering vector $q_x \sim \pi/8$ [40]. Similar scattering vectors have been reported earlier in FeSe as well as $FeSe_{0.4}Te_{0.6}$ [39]. Thus, our results show good agreement with the experiments. The dependence of the QPI pattern on the quasiparticle energy is similar in various aspects to that in the nematic state.

QPI patterns obtained for energy $\omega = -100$ meV in the SDW state as shown in Figs. 4(d)–4(i) are the central results of this work. The dominant effect of the OS term can be easily seen even though there is significant reconstruction of the band structure. The band retains the salient features of the nematic state and shows only a little change with temperature. Consequently, the LDOS modulation is nearly 1D with orientation along the antiferromagnetic direction [Figs. 4(g)–4(i)]. Similarly, the momentum-space QPI patterns consist of parallel running peak structures in a direction reciprocal to the ferromagnetic direction. An additional negative peak structure is present in between the two. All of these characteristics are in excellent agreement with the STM results, including a small change with the temperature. The latter can be seen from the fact that there is only a little change in the scattering vector magnitude as a function of quasiparticle energy (see Fig. 5).

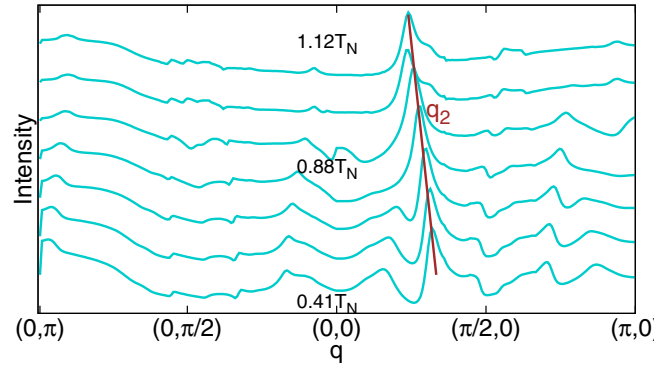

FIG. 5. QPI along the high-symmetry directions in the SDW state for different temperatures, starting from $T = 0.014t$ (bottom curve) to $T = 0.036t$ (top curve) with steps of $0.04t$ ($T_N \approx 0.034t$). The brown curve is a guide to the eye for scattering vector $\mathbf{q}_2$.

Similar QPI patterns have been observed in the SDW state of $Ca(Fe_{1-x}Co_x)_2As_2$ [7,19] and NaFeAs [20]. The wavelengths for 1D LDOS modulation in the two pnictides are $\approx 8a_{\text{Fe-Fe}}$ and $\approx 13a_{\text{Fe-Fe}}$, respectively, which compares well with $\sim 8a_{\text{Fe-Fe}}$ obtained within the five-orbital of Ref. [34] considered in this work (see Table I).

Finally, we should note that if the OS between the d_{xz} and d_{yz} orbitals is reversed ($\delta \to -\delta$), the QPI patterns in the pure SC state or in the nematic state get rotated by $\pi/2$ for the same energy. However, its effect is nontrivial in the SDW state because it involves a significant reconstruction of the electronic structure. Also, we find that the patterns lose the 1D characteristics, which is otherwise strongly favored when the orbital d_{xz} is lower in energy (see Supplemental Material [38] for more details).

To conclude, the occurrence of parallel rodlike structures in the momentum space QPI or 1D spatial modulation of the LDOS in various phases of pnictides and chalcogenides is an indication of a common factor at play. We identify this as a symmetry-breaking term involving nondegenerate d_{xz} and d_{yz} orbitals. Incorporating such a term while considering different phases, we have obtained all the essential features of QPI patterns and particularly the 1D LDOS modulations. In addition, we find it crucial that the energy of the d_{xz} orbital be lower so that the orientation of anisotropic structures is robust against the change in quasiparticle energy. It is also illustrated how the nonuniform spectral density distribution along the constant energy contours, because of the nearby band extrema, leads to highly anisotropic impurity scattering.

TABLE I. Size of one-dimensional nanostructures in the LDOS modulation of various iron-based superconductors. We obtain the length scale of the LDOS modulation $\sim 6a$–$11a$.

Phase	Nematic	SDW	SC
$Ca(Fe_{1-x}Co_x)_2As_2$ [7,19]		$8a$	
NaFeAs [20]	$13a$	$13a$	
FeSe [10,11,39]			$16a$

We are grateful to P. Wahl, S. Wirth, S. Rößler, S. Borisenko, Z. Sun, Y. Bang, and I. Eremin for fruitful discussions. We acknowledge the use of HPC cluster at HRI. A.A. acknowledges support through National Research Foundation of Korea (NRF) funded by the Ministry of Science of Korea (Grants No. 2015R1C1A1A01052411 and No. 2017R1D1A1B03033465), and by the National Foundation of Korea (NRF) funded by the Ministry of Science, ICT and Future Planning (No. 2016K1A4A4A01922028).

[1] G. R. Stewart, Rev. Mod. Phys. **83**, 1589 (2011).
[2] J.-H. Chu, J. G. Analytis, K. De Greve, P. L. McMahon, Z. Islam, Y. Yamamoto, and I. R. Fisher, Science **329**, 824 (2010).
[3] M. A. Tanatar, E. C. Blomberg, A. Kreyssig, M. G. Kim, N. Ni, A. Thaler, S. L. Bud'ko, P. C. Canfield, A. I. Goldman, I. I. Mazin, and R. Prozorov, Phys. Rev. B **81**, 184508 (2010).
[4] E. C. Blomberg, M. A. Tanatar, R. M. Fernandes, I. I. Mazin, B. Shen, H.-H. Wen, M. D. Johannes, J. Schmalian, and R. Prozorov, Nat. Commun. **4**, 1914 (2013).
[5] M. Nakajima, T. Liang, S. Ishida, Y. Tomioka, K. Kihou, C. H. Lee, A. Iyo, H. Eisaki, T. Kakeshita, T. Ito, and S. Uchida, Proc. Natl. Acad. Sci. USA **108**, 12238 (2011).
[6] M. Yi, D. Lu, J.-H. Chu, J. G. Analytis, A. P. Sorini, A. F. Kemper, B. Moritz, S.-K. Mo, R. G. Moore, M. Hashimoto, W.-S. Lee, Z. Hussain, T. P. Devereaux, I. R. Fisher, and Z.-X. Shen, Proc. Natl. Acad. Sci. USA **108**, 6878 (2011).
[7] T.-M. Chuang, M. P. Allan, J. Lee, Y. Xie, N. Ni, S. L. Bud'ko, G. S. Boebinger, P. C. Canfield, and J. C. Davis, Science **327**, 181 (2010).
[8] H. Kontani, Y. Inoue, T. Saito, Y. Yamakawa, and S. Onari, Solid State Commun. **152**, 718 (2012).
[9] S. Kasahara, H. J. Shi, K. Hashimoto, S. Tonegawa, Y. Mizukami, T. Shibauchi, K. Sugimoto, T. Fukuda, T. Terashima, A. H. Nevidomskyy, and Y. Matsuda, Nature (London) **486**, 382 (2012).
[10] C.-L. Song, Y.-L. Wang, P. Cheng, Y.-P. Jiang, W. Li, T. Zhang, Z. Li, K. He, L. Wang, J.-F. Jia, H.-H. Hung, C. Wu, X. Ma, X. Chen, and Q.-K. Xue, Science **332**, 1410 (2011).
[11] C.-L. Song, Y.-L. Wang, Y.-P. Jiang, L. Wang, K. He, X. Chen, J. E. Hoffman, X.-C. Ma, and Q.-K. Xue, Phys. Rev. Lett. **109**, 137004 (2012).
[12] T. Shimojima, Y. Suzuki, T. Sonobe, A. Nakamura, M. Sakano, J. Omachi, K. Yoshioka, M. Kuwata-Gonokami, K. Ono, H. Kumigashira, A. E. Böhmer, F. Hardy, T. Wolf, C. Meingast, H. v. Löhneysen, H. Ikeda, and K. Ishizaka, Phys. Rev. B **90**, 121111 (2014).
[13] K. Nakayama, Y. Miyata, G. N. Phan, T. Sato, Y. Tanabe, T. Urata, K. Tanigaki, and T. Takahashi, Phys. Rev. Lett. **113**, 237001 (2014).
[14] M. D. Watson, T. K. Kim, A. A. Haghighirad, N. R. Davies, A. McCollam, A. Narayanan, S. F. Blake, Y. L. Chen, S. Ghannadzadeh, A. J. Schofield, M. Hoesch, C. Meingast, T. Wolf, and A. I. Coldea, Phys. Rev. B **91**, 155106 (2015).
[15] S.-H. Baek, D. V. Efremov, J. M. Ok, J. S. Kim, J. van den Brink, and B. Büchner, Nat. Mater. **14**, 210 (2014).
[16] P. Zhang, T. Qian, P. Richard, X. P. Wang, H. Miao, B. Q. Lv, B. B. Fu, T. Wolf, C. Meingast, X. X. Wu, Z. Q. Wang, J. P. Hu, and H. Ding, Phys. Rev. B **91**, 214503 (2015).
[17] Y. Suzuki, T. Shimojima, T. Sonobe, A. Nakamura, M. Sakano, H. Tsuji, J. Omachi, K. Yoshioka, M. Kuwata-Gonokami, T. Watashige, R. Kobayashi, S. Kasahara, T. Shibauchi, Y. Matsuda, Y. Yamakawa, H. Kontani, and K. Ishizaka, Phys. Rev. B **92**, 205117 (2015).
[18] J. E. Hoffman, Rep. Prog. Phys. **74**, 124513 (2011); D. Huang, T. A. Webb, S. Fang, C.-L. Song, C.-Z. Chang, J. S. Moodera, E. Kaxiras, and J. E. Hoffman, Phys. Rev. B **93**, 125129 (2016); T. Hanaguri, S. Niitaka, K. Kuroki, and H. Takagi, Science **328**, 474 (2010); P. J. Hirschfeld, D. Altenfeld, I. Eremin, and I. I. Mazin, Phys. Rev. B **92**, 184513 (2015); P. O. Sprau, A. Kostin, A. Kreisel, A. E. Böhmer, V. Taufour, P. C. Canfield, S. Mukherjee, P. J. Hirschfeld, B. M. Andersen, and J. C. S. Davis, Science **357**, 75 (2017); J. Böker, P. A. Volkov, K. B. Efetov, and I. Eremin, Phys. Rev. B **96**, 014517 (2017); D. K. Singh and P. Majumdar, *ibid.* **96**, 235111 (2017); J. H. J. Martiny, A. Kreisel, P. J. Hirschfeld, and B. M. Andersen, *ibid.* **95**, 184507 (2017); D. Altenfeld, P. J. Hirschfeld, I. I. Mazin, and I. Eremin, *ibid.* **97**, 054519 (2018); B. Kamble, A. Akbari, and I. Eremin, Europhys. Lett. **114**, 17001 (2016); Z. Du, X. Yang, D. Altenfeld, Q. Gu, H. Yang, I. Eremin, P. J. Hirschfeld, I. I. Mazin, H. Lin, X. Zhu, and H.-H. Wen, Nat. Phys. **14**, 134 (2017); S. Choi, S. Johnston, W.-J. Jang, K. Koepernik, K. Nakatsukasa, J. M. Ok, H.-J. Lee, H. W. Choi, A. T. Lee, A. Akbari, Y. K. Semertzidis, Y. Bang, J. S. Kim, and J. Lee, Phys. Rev. Lett. **119**, 107003 (2017); S. Sykora and P. Coleman, Phys. Rev. B **84**, 054501 (2011); D. K. Singh, Phys. Lett. A **381**, 2761 (2017); A. Kostin, P. O. Sprau, A. Kreisel, Y. X. Chong, A. E. Böhmer, P. C. Canfield, P. J. Hirschfeld, B. M. Andersen, and J. C. S. Davis, Nat. Mater. **17**, 869 (2018).
[19] M. P. Allan, T.-M. Chuang, F. Massee, Y. Xie, N. Ni, S. L. Bud'ko, G. S. Boebinger, Q. Wang, D. S. Dessau, P. C. Canfield, M. S. Golden, and J. C. Davis, Nat. Phys. **9**, 220 (2013).
[20] E. P. Rosenthal, E. F. Andrade, C. J. Arguello, R. M. Fernandes, L. Y. Xing, X. C. Wang, C. Q. Jin, A. J. Millis, and A. N. Pasupathy, Nat. Phys. **10**, 225 (2014).
[21] E. Bascones, B. Valenzuela, and M. J. Calderón, Phys. Rev. B **86**, 174508 (2012).
[22] J. Knolle, I. Eremin, A. Akbari, and R. Moessner, Phys. Rev. Lett. **104**, 257001 (2010); A. Akbari, J. Knolle, I. Eremin, and R. Moessner, Phys. Rev. B **82**, 224506 (2010).
[23] I. I. Mazin, S. A. J. Kimber, and D. N. Argyriou, Phys. Rev. B **83**, 052501 (2011).
[24] N. Plonka, A. F. Kemper, S. Graser, A. P. Kampf, and T. P. Devereaux, Phys. Rev. B **88**, 174518 (2013).
[25] H.-Y. Zhang and J.-X. Li, Phys. Rev. B **94**, 075153 (2016).
[26] C. Fang, H. Yao, W.-F. Tsai, J. P. Hu, and S. A. Kivelson, Phys. Rev. B **77**, 224509 (2008).
[27] R. M. Fernandes, A. V. Chubukov, J. Knolle, I. Eremin, and J. Schmalian, Phys. Rev. B **85**, 024534 (2012).
[28] R. M. Fernandes, A. V. Chubukov, and J. Schmalian, Nat. Phys. **10**, 97 (2014); R. M. Fernandes, L. H. VanBebber, S. Bhattacharya, P. Chandra, V. Keppens, D. Mandrus,

M. A. McGuire, B. C. Sales, A. S. Sefat, and J. Schmalian, Phys. Rev. Lett. **105**, 157003 (2010).

[29] F. Krüger, S. Kumar, J. Zaanen, and J. van den Brink, Phys. Rev. B **79**, 054504 (2009).

[30] W. Lv, J. Wu, and P. Phillips, Phys. Rev. B **80**, 224506 (2009); W. Lv, F. Krüger, and P. Phillips, *ibid.* **82**, 045125 (2010).

[31] C.-C. Lee, W.-G. Yin, and W. Ku, Phys. Rev. Lett. **103**, 267001 (2009).

[32] S. Onari and H. Kontani, Phys. Rev. Lett. **109**, 137001 (2012); H. Kontani and Y. Yamakawa, *ibid.* **113**, 047001 (2014); Y. Yamakawa, S. Onari, and H. Kontani, Phys. Rev. X **6**, 021032 (2016).

[33] S. S. Dhesi, A. Mirone, C. De Nadaï, P. Ohresser, P. Bencok, N. B. Brookes, P. Reutler, A. Revcolevschi, A. Tagliaferri, O. Toulemonde, and G. van der Laan, Phys. Rev. Lett. **92**, 056403 (2004).

[34] H. Ikeda, R. Arita, and J. Kuneš, Phys. Rev. B **81**, 054502 (2010).

[35] X. Liu, R. Tao, M. Ren, W. Chen, Q. Yao, T. Wolf, Y. Yan, T. Zhang, and D. Feng, arXiv:1803.07304.

[36] Y.-Y. Zhang, C. Fang, X. Zhou, K. Seo, W.-F. Tsai, B. A. Bernevig, and J. Hu, Phys. Rev. B **80**, 094528 (2009).

[37] C. de la Cruz, Q. Huang, J. W. Lynn, J. Li, W. Ratcliff II, J. L. Zarestky, H. A. Mook, G. F. Chen, J. L. Luo, N. L. Wang, and P. Dai, Nature (London) **453**, 899 (2008).

[38] See Supplemental Material at http://link.aps.org/supplemental/10.1103/PhysRevB.98.180506 for the methods used in calculating quasiparticle interference patterns of the superconducting or spin-density-wave state and also for the dependence of patterns on the order parameters or nature of orbital-splitting.

[39] U. R. Singh, S. C. White, S. Schmaus, V. Tsurkan, A. Loidl, J. Deisenhofer, and P. Wahl, Sci. Adv. **1**, e1500206 (2015).

[40] T. Hanaguri, K. Iwaya, Y. Kohsaka, T. Machida, T. Watashige, S. Kasahara, T. Shibauchi, and Y. Matsuda, Sci. Adv. **4**, eaar6419 (2018).